

## Article

# Preparation of Cold Sprayed Titanium TA2 Coating by Irregular Powder and Evaluation of Its Corrosion Resistance

Zhengyi Li <sup>1</sup> , Na Wang <sup>2</sup>, Shuhua Li <sup>3</sup>, Lei Wen <sup>1</sup>, Chengcheng Xu <sup>1,4,\*</sup>  and Dongbai Sun <sup>1,5,\*</sup>

<sup>1</sup> National Center for Materials Services Safety, University of Science and Technology Beijing, Beijing 100083, China; zy370983@163.com (Z.L.); wenlei@ustb.edu.cn (L.W.)

<sup>2</sup> The Second Gas Production Plant of Changqing Oilfield Branch, China National Petroleum Corporation, Yulin 719000, China; wangn1\_cq@petrochina.com.cn

<sup>3</sup> Gas Field Development Department of Changqing Oilfield Branch, China National Petroleum Corporation, Xi'an 710018, China; lishuhua@petrochina.com.cn

<sup>4</sup> Shenzhen National High-Tech Industry Innovation Center, Shenzhen 518063, China

<sup>5</sup> Materials Science and Engineering, Sun Yat-sen University, Guangzhou 510275, China

\* Correspondence: hotxcc@126.com (C.X.); sundongbai@mail.sysu.edu.cn (D.S.);

Tel.: +86-18680685622 (C.X.); +86-13701062655 (D.S.)

**Abstract:** Titanium coating on a steel substrate by surface technology can improve the corrosion resistance of steel. In this paper, the titanium TA2 coating was deposited on X80 steel by cold spraying equipment with a low-cost irregular powder. The effects of the carrier gas temperature on the microstructure, microhardness, wear resistance, adhesion and corrosion resistance of titanium coatings, especially in a deep sea environment, were studied by methods of porosity analysis, thermal field emission scanning analysis, energy spectrum analysis, Vickers hardness tests, bonding strength tests, friction and wear tests and electrochemical tests. The results showed that as the carrier gas temperature increased from 300 °C to 900 °C, the porosity of the coating decreased to 0.93%, and the hardness and bonding strength of the coating increased to 247 HV<sub>0.5</sub> and 46.7 MPa, respectively. With the increase in hydrostatic pressure from 0.1 MPa to 40 MPa, the dimensional blunt current density of the titanium coating with 0.93% porosity was still in the order of 10<sup>-7</sup> A·cm<sup>-2</sup> with the cast titanium TA2.

**Keywords:** titanium coating; cold spraying; corrosion resistance; marine



**Citation:** Li, Z.; Wang, N.; Li, S.; Wen, L.; Xu, C.; Sun, D. Preparation of Cold Sprayed Titanium TA2 Coating by Irregular Powder and Evaluation of Its Corrosion Resistance. *Coatings* **2023**, *13*, 1894. <https://doi.org/10.3390/coatings13111894>

Academic Editor: Lubomír Čaplovič

Received: 25 September 2023

Revised: 17 October 2023

Accepted: 25 October 2023

Published: 4 November 2023



**Copyright:** © 2023 by the authors. Licensee MDPI, Basel, Switzerland. This article is an open access article distributed under the terms and conditions of the Creative Commons Attribution (CC BY) license (<https://creativecommons.org/licenses/by/4.0/>).

## 1. Introduction

Deep sea environment service conditions are very harsh. The traditional organic heavy anticorrosion coatings can easily fall off and have poor mechanical properties, poor wear resistance and other shortcomings, which makes it difficult for them to withstand impacts and friction [1–3]. For marine environments, anticorrosion, seawater erosion resistance and good mechanical properties are the most important characteristics of marine equipment materials. Titanium, titanium alloys and titanium-based cemented carbide have low density, high strength and excellent seawater corrosion resistance [4–6], but the high cost limits their application. By depositing titanium and titanium alloy coatings on iron and steel materials through advanced surface treatment technology to replace titanium and titanium alloy materials, one can significantly reduce the application costs and achieve the corrosion resistance effect of titanium alloy. Porosity is a key performance index for the protective coating serving in the deep sea environment. Seawater can direct the substrate along the pores of the coating, forming corrosion and diffusion, resulting in the coating's failure [7–9]. Thermal sprayed coatings generally have high porosity and oxidation levels and residual stress problems [10–12]. The reason is that titanium can easily react with oxygen at higher temperatures, which is converted into oxides, nitrides and carbides during the spraying process [13], resulting in the high porosity of the coating. Vacuum plasma spraying and

supersonic plasma spraying were used to solve the problem of the reaction between the titanium and gas in the spraying process [14,15]. Compared with the thermal sprayed coating, the cold sprayed coating had very low porosity, a low oxidation degree and thermal stress. The cold spraying method can be used to prepare metal coatings, cermet coatings and amorphous and nanostructured metal coatings [16–21]. Cold spraying requires good shear instability between the powder and matrix [22]. The key to forming a good coating deposition effect is the collision velocity between the spraying particles and the substrate, which is affected by many factors, such as the carrier temperature, carrier gas pressure, spraying distance and particle shape and size [23,24]. The cold spraying temperature affects the velocity of powder particles in the spraying process. When the temperature and pressure of the gas increase, the velocity of the particles increases, and the porosity of the coating decreases [23]. However, when the spraying temperature exceeds the melting point of the powder, intermetallic compounds will form at the interface, resulting in a reduction in interface bonding strength; when spraying at a non-vertical angle, the combination of particles and the matrix will be weakened [25]. A few pores at the interface between the cold sprayed coating and the substrate are caused by the sputtering effect of the substrate on the powder particles [26]. When the pressure of the powder feeding gas is small and the temperature is low, the sputtering effect is particularly obvious. Wong et al. [23] used spherical and irregular titanium powder to prepare a cold spray coating. The results showed that the coating prepared with the irregular powder was denser, because the drag constant of irregular particles was higher, and a higher particle velocity could be obtained at the nozzle outlet, but the irregular powder was more likely to oxidize in the spraying process [27]. By comprehensively comparing the critical velocity and density, Wong et al. [28] found that the spherical medium-sized spherical titanium powder was the most suitable for cold spraying.

Some scholars have also attempted to improve the overall performance of titanium and titanium alloy coatings by auxiliary means, such as solid solution treatment, heat treatment, substrate preheating, hot isostatic pressing treatment, etc. The significant change in the surface morphology and the increase in the residual stress level of the coating depend on the interaction time of the laser beam [29]. The bonding strength of the cold sprayed coating can be improved by solid solution and aging treatment [30]. Preheating the substrate before cold spraying can effectively reduce the porosity of the coating to less than 1% [31]. The performance of titanium and titanium coatings has also been the focus of attention [32–37]. Kinoshita et al. used electrochemical methods to test the corrosion performance of plasma sprayed titanium coatings in a NaCl solution. The results showed that the porosity of the coating significantly accelerated the corrosion of the steel substrate. Wang et al. found that a low-porosity coating is beneficial to reduce the corrosion current density of the coating and improve the corrosion resistance of the coating. Wen Sun et al. [38,39] evaluated the bonding strength, electrochemical properties and wear resistance of a TC4 coating and found that they were better than those of a TC4 substrate.

To obtain a good cold spraying effect, titanium and titanium alloy coatings are usually prepared from a spherical powder after plasma spheroidization or atomization. The processing of spherical powders is complex, and the cost of titanium coatings can be effectively reduced by directly using irregular and non-spheroidized irregular powders. However, there are few reports on the preparation of titanium coatings using irregular powders. At the same time, the performance of titanium coatings in marine environments is neglected in the research, especially the influence of deep sea hydrostatic pressure on titanium coatings. Therefore, this paper focuses on the preparation of a titanium coating with an irregular powder and the evaluation of its performance. In this work, the cold sprayed titanium coatings were prepared on the surface of X80 steel with the carrier gas temperature as the control parameter and irregular titanium powder as the raw material. The comprehensive properties of the coatings were characterized by the porosity, bonding strength, XRD, hardness, electrochemical properties, wear resistance and other indicators.

The effects of deep sea hydrostatic pressure on the electrochemical properties and failure behavior of the coatings were studied.

## 2. Materials and Methods

### 2.1. Materials

The substrate was hot-rolled X80 pipeline steel, the coating was deposited on sodium reduction sponge titanium TA2 powder after crushing, and its composition is shown in Table 1. The X80 steel was processed into a plate-like specimen with a size of 80 mm × 100 mm × 4 mm and sandblasted. The morphology of the pure titanium powder used in the cold spraying test is shown in Figure 1a,b. It can be seen from the figure that the titanium powder used for spraying had irregular polygonal particles with good dispersion. A laser particle size analyzer (CLF-2 Malvern Panalytical, Hegeney, UK) was used to analyze the particle size. Figure 1c shows that the particle size of the pure titanium powders was concentrated in the 20–60 μm range.

**Table 1.** The components of X80 pipe steel and TA2 titanium powder, wt.%.

Element	C	Mn	Cr	Mo	Cu	Ni	Si	Nb	Al	Fe
X80 steel	0.065	2.041	0.329	0.229	0.229	0.184	0.148	0.084	0.024	Bal.
Element	C	N	H	Fe	O	Ti				
TA2 titanium powder	0.069	0.025	0.012	0.330	0.213	Bal.				

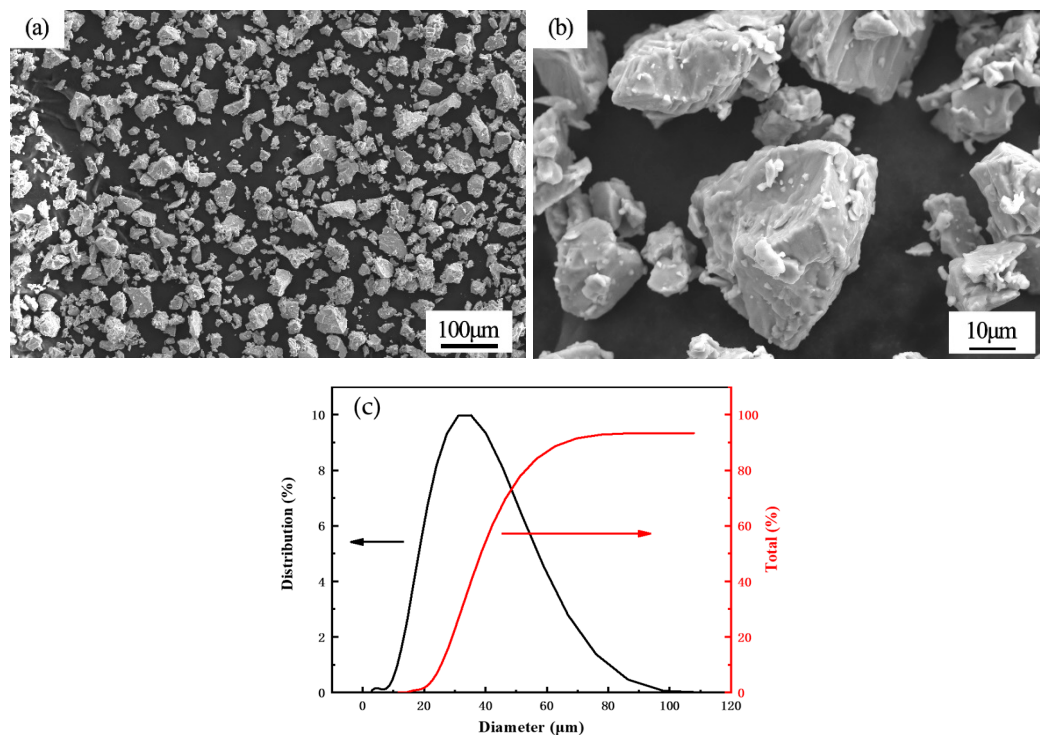


**Figure 1.** (a) The macroscopic morphology of titanium TA2 powder; (b) the microstructure of titanium TA2 powder; (c) powder size distribution.

### 2.2. Preparation of Cold Sprayed Titanium Coatings

In this cold spraying test, the coating was prepared at a constant air source pressure and different carrier gas temperatures (300, 500, 700, and 900 °C) as the adjustable parameter, and the pressure of the powder carrier gas was set to 5 MPa. The coating was prepared by the cold spraying system (PCS-1000, Plasma Giken Co., Ltd., Saitama, Japan). The parameters of the cold spraying system are shown in Table 2. The pores of the metal

coating could become a channel for seawater to penetrate the coating/substrate interface. Thus, a galvanic corrosion situation with a large cathode (titanium coating) and a small anode (substrate exposure position) could be formed. This could accelerate the substrate's corrosion. It was necessary to seal the coating to solve the problem of pores in the coating [40]. In this study, stearic acid was used to seal the cold sprayed titanium coating. The sealing process was as follows: a 0.01 mol/L stearic acid ethanol solution was prepared; the titanium coating was placed in the solution for 10 h; after removal, it was placed in the oven at 60 °C for 1 h to complete the sealing.

**Table 2.** The parameters of cold spraying.

Specimen	Temperature, °C	Gas	Pressure, MPa	Velocity, m/s	Swing Speed, cm/s	Powder Feed Rate, g/min
C1	300	N <sub>2</sub>	4.5	681	1	20
C2	500	N <sub>2</sub>	4.5	753	1	20
C3	700	N <sub>2</sub>	4.5	812	1	20
C4	900	N <sub>2</sub>	4.5	862	1	20

### 2.3. Characterization of Cold Sprayed Titanium Coatings

After the coating preparation, 10 electron microscopy photos of the coating section morphology were selected, and the porosity of the coating section was analyzed with the ImagePro plus 6.0 software (Media Cybernetic, St. Petersburg, FL, USA). Bonding strength, microhardness and friction and wear tests were carried out on the coating to characterize its mechanical properties. The size of the bonding strength sample was  $\varphi$  25 mm  $\times$  3 mm, and it was tested according to ASTM C633-01 [41]. The friction and wear test was carried out on the friction and wear testing machine (RTEC MFT5000, San Jose, CA, USA). The friction form was reciprocating friction, the friction frequency was 50 Hz, the friction pair was an aluminum oxide ball with a 6 mm diameter, and the loading load was 20 N. A laser confocal microscope (Olympus LEXT OLS4100, Tokyo, JAP) was used to observe the surface morphology of the coating after friction and wear, and the cross-sectional size of the wear marks was measured. Scanning electron microscopy (SEM, FEI Quanta 650F, Hillsboro, OR, USA) was used to observe the morphology of the coating cross-section. Energy-dispersive X-ray spectroscopy (EDS, QUASOR, Waltham, MA, USA) was used to analyze the elemental distribution of the coating cross-section.

### 2.4. Assessment of Service Performance

The multi-factor coupled environmental simulation test device of the research group (Figure 2) was used to conduct service evaluation experiments. The experimental device controls the chemical environment of the solution in the autoclave through two circuits: a hydrochemical control loop and a pressure control loop. The dissolved oxygen control system is connected to the 10 L main tank. The system controls the input of oxygen and nitrogen from the air source to the main tank through the feedback of the dissolved oxygen sensor and the solenoid valve, to accurately control the dissolved oxygen content in the main tank. The pressure control circuit passes the solution in the reservoir through the diaphragm pump to increase the hydrostatic pressure in the autoclave, after which the solution reduces the pressure through the back pressure valve and returns to the main tank. The temperature control system controls the temperature of the solution via a heating/insulation shell or cooling devices. The device can simultaneously control the chemical and environmental parameters of the water, such as the pressure, temperature, dissolved oxygen concentration and pH value. Moreover, in situ electrochemical testing was carried out under a high-pressure environment. The pressure control range of the device was 0.1–50 MPa, realizing the simulation of a deep sea environment equivalent to the depth of 5000 m. The temperature control range was 0–120 °C, the dissolved oxygen concentration control range was 0.3–20 ppm, and the pH value control range was 0–14. The

experimental device controlled the chemical environment of the solution in the autoclave through two circuits to simulate the real marine environment: the water chemistry control loop and the high pressure circulation loop. The hydrostatic pressure of this experiment was set to four pressure gradients of 0.1, 10, 20, and 40 MPa. The experimental temperature was 5 °C, the pH value of the solution was 7.0, and the dissolved oxygen concentration was 3.8 ppm.

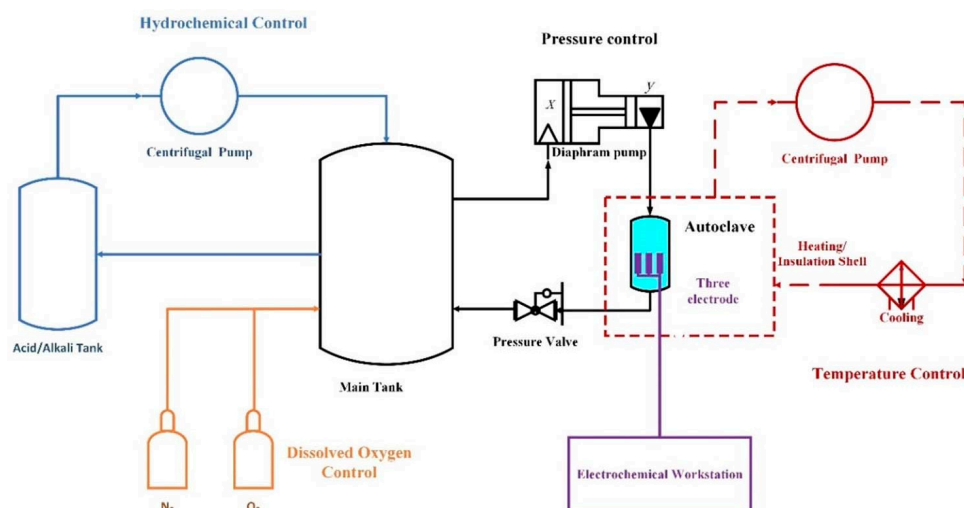


**Figure 2.** The schematic diagram of the multi-factor coupled environment simulation test device.

The electrochemical tests were performed on an electrochemical workstation (AMETK P4000, San Diego, CA, USA) using a three-electrode system: a reference electrode (the solid Ag/AgCl electrode), a platinum mesh electrode, and a coated working electrode. The coating layer was the test surface, the back of the substrate was brazed to the copper wire link, and the sample was sealed with epoxy resin. The test surface was sanded with 200#, 400#, 600#, 800#, 1000#, 1500#, and 2000# sandpapers in turn. Before the electrochemical test, the surface of the sample was cleaned and blown dry with distilled water, acetone, and alcohol.

### 3. Results and Discussion

#### 3.1. Changes in the Microstructure of Cold Sprayed Titanium Coatings

The micromorphology of titanium coatings cold sprayed under different carrier gas temperatures and process conditions is shown in Figure 3. Under the four process conditions, the coating thickness was not consistent. This means that less powder was effectively deposited under the process conditions of a lower carrier gas temperature, leading to a difference in deposition efficiency under different carrier gas temperatures. As can be seen from the figure, the microstructures of the C1 (300 °C) and C2 (500 °C) coatings showed a porous top layer of 150 µm and a lower layer of higher porosity. The bottom layer porosity of the C3 (700 °C) coating was relatively small, and the top layer porosity was also significantly reduced. The top porous layer of the C4 (900 °C) coating was not obvious, and the bottom layer had no porosity. The formation of the porous top layer of the cold sprayed titanium coating was due to the cumulative densification effect [42] caused by the continuous impact of powder particles during the cold spraying process. At the bottom of the coating, the powder particles impacted the substrate surface to produce violent plastic deformation, produce mechanical bonding with the substrate, and deposit to form the coating. Due to the continuous impact of subsequent particles, the deposited coating experienced a strong tamping effect and produced a large deformation to eliminate the gaps between particles. Meanwhile, the continuous impact of subsequent particles also formed a micro-forging effect on the surface to improve the strength [43] of the coating.

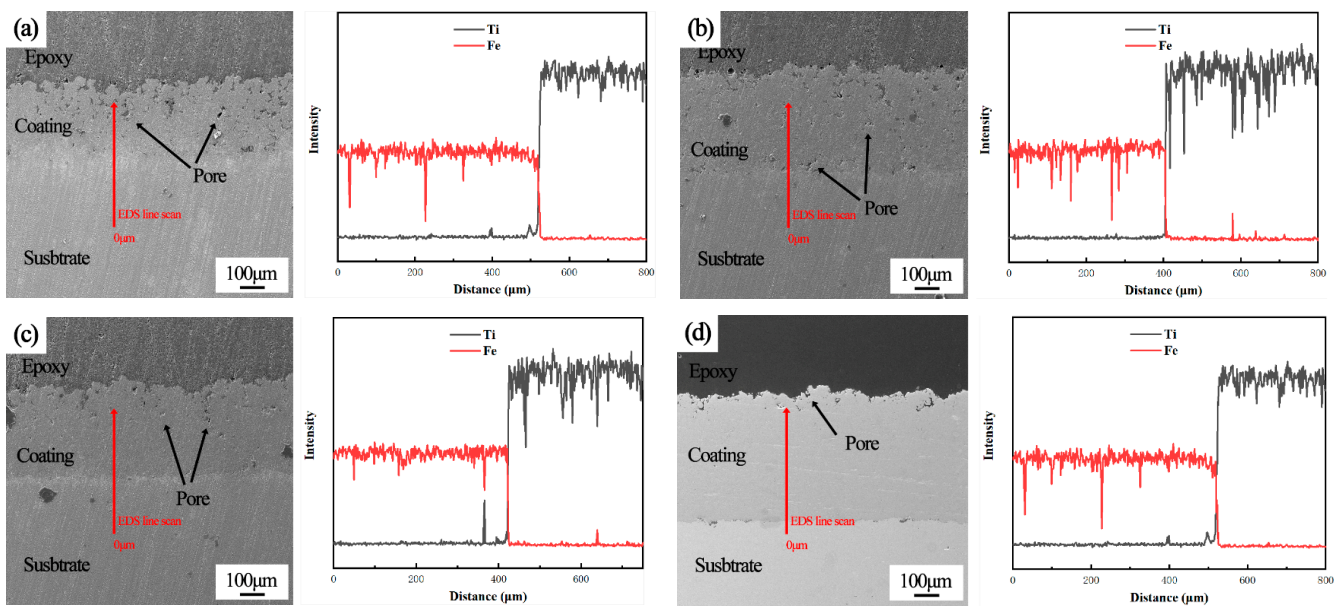


**Figure 3.** The micromorphology and cross-section element distribution of coatings with different carrier gas temperatures: (a) 300 °C; (b) 500 °C; (c) 700 °C; (d) 900 °C.

As can be seen from Figure 3, the carrier gas temperature had a great influence on the coating's porosity. The porosity of the coating section (including the top porous layer) prepared under different spraying conditions was statistically analyzed, and the statistical results are shown in Figure 4. The porosity of the C1 coating was 7.53%, while that of the C4 coating was only 0.93%. The porosity of the coating decreased with the carrier gas temperature increase. In the cold spraying process, a carrier gas temperature increase will render the particles more likely to deform during the spraying process. At the same time, the temperature increase will increase the spraying gas speed, and the particle speed will be higher [44]. Thus, the compaction effect of the coating deposition process would be better and more dense.

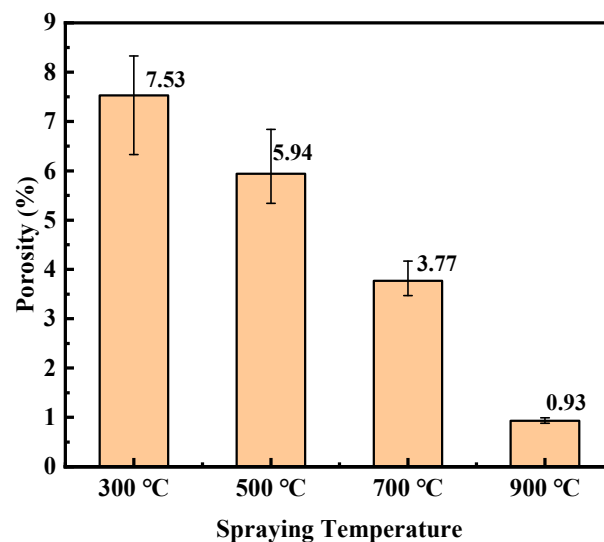


**Figure 4.** Porosity statistics of titanium coatings at different carrier gas temperatures.

Increasing temperatures will accelerate the oxidation of particles and generate titanium oxide, nitride, and carbide, thus reducing the bonding strength between coating particles. Therefore, X-ray diffraction (XRD) tests were carried out on the original titanium powder and the coatings prepared under different spraying conditions to characterize the phase

changes, and the results are given in Figure 5. It can be seen from the results that the phase of the titanium coating did not change and no new phase was generated. This indicates that the titanium powder was deposited in the form of mechanical bonding. Compared with the titanium powder, the diffraction peak of Fe was observed in the diffraction results of the C1 coating. The Fe diffraction peak was not observed in the test results of the C2, C3, and C4 coatings. The strength and half-height width of the diffraction peak of the coating were different from those of the titanium powder. This is mainly because the impact deformation of titanium powder during cold spraying will lead to grain fragmentation, leading to a difference in the strength and half-height width of the coating's diffraction peak.

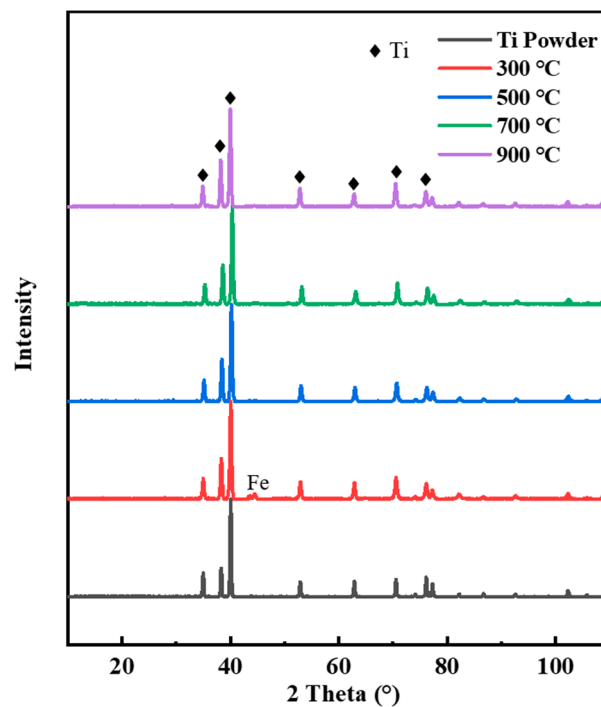


**Figure 5.** XRD spectra of titanium coatings with different carrier gas temperatures.

### 3.2. Properties of Cold Sprayed Titanium Coatings

Bond strength is a key index affecting the use of coatings, and the results are shown in Figure 6a. With the temperature increase, the bonding strength of the coating increased from 8.7 MPa at 300 °C to 46.7 MPa at 900 °C. The hardness can reflect the wear resistance of the coating to a certain extent. The hardness test results are shown in Figure 6b. With the carrier gas temperature increment, the hardness increased, and the hardness values of the C1, C2, C3, and C4 coatings were 126, 166, 185, and 247 HV<sub>0.5</sub>, respectively. In the cold spraying process, the higher carrier gas temperature represents a higher particle speed. At a higher particle speed, the impact of the particles on the substrate will lead to more plastic deformation and strengthen the mechanical bonding effect, thus improving its bond strength and hardness.

Wear resistance is another key performance aspect of the coating in service, and the wear test results of the coatings are shown in Figure 7. The wear area of the coating decreased with the carrier gas temperature increment; the wear area of the C1 coating was 4.14  $\mu\text{m}^2$ , and that of the C4 coating was reduced to 1.26  $\mu\text{m}^2$ .

From the perspective of wear morphology, the main form of coating friction under different process conditions was abrasive wear, accompanied by stripping wear. In the wear morphology of the C1 coating, there were large peeling wear traces and titanium powder with insufficient deformation under the peeling layer. However, only small pieces of the peeling layer were found on the C2 and C3 coatings, while no peeling layer wear was found on the C4 coating; only abrasive wear characteristics were found.

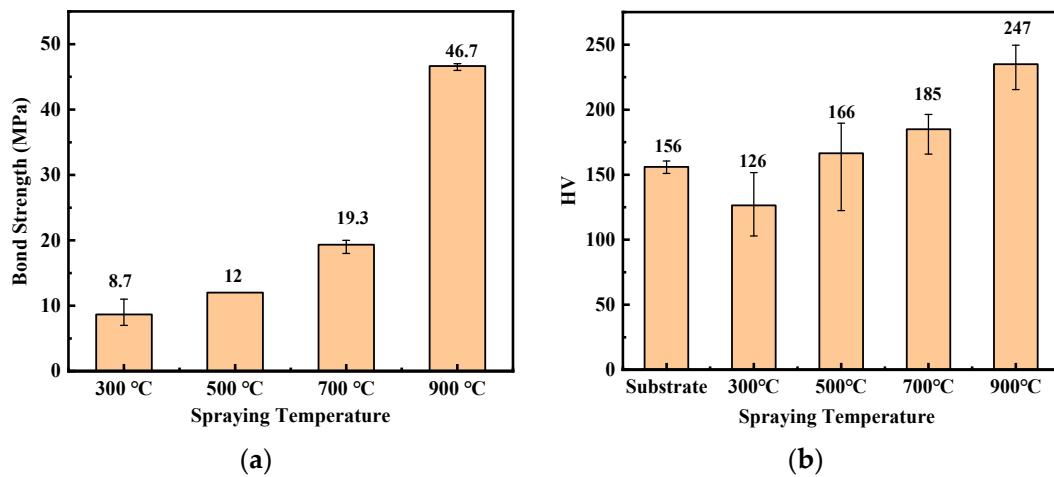


Figure 6. Titanium coatings with different spray processes: (a) bond strength and (b) hardness.

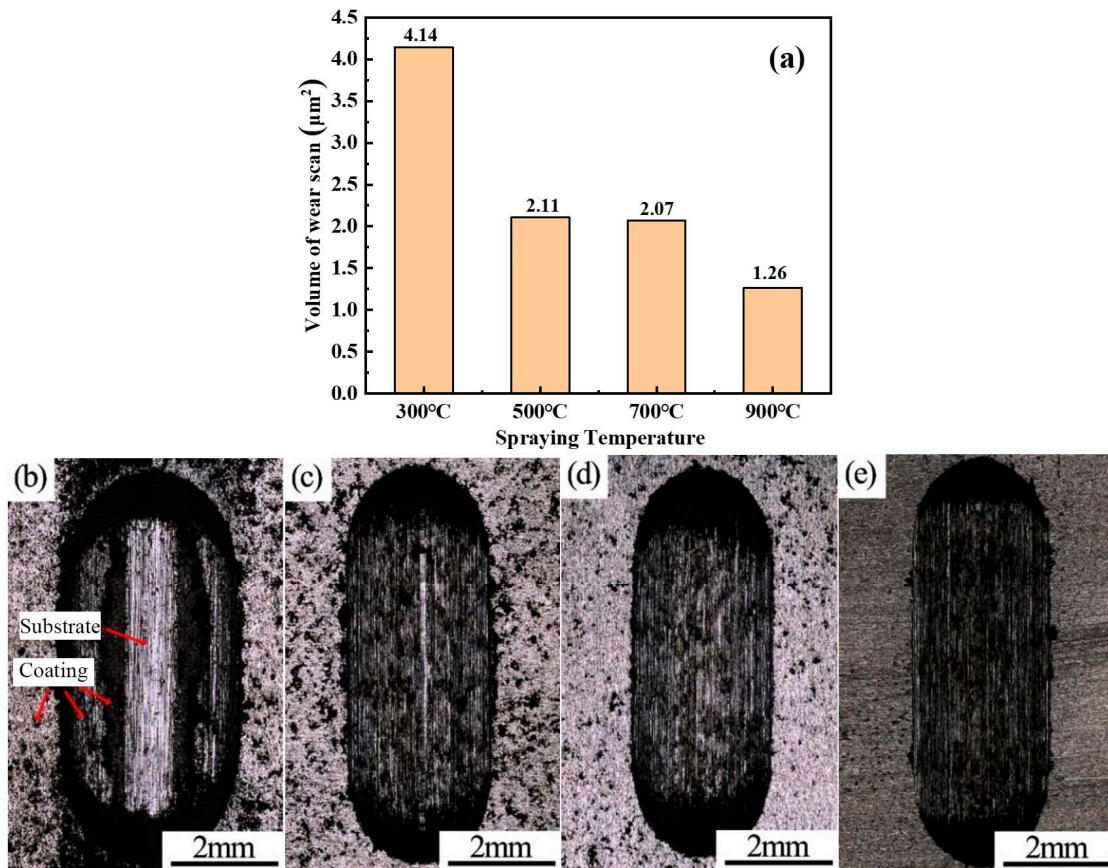
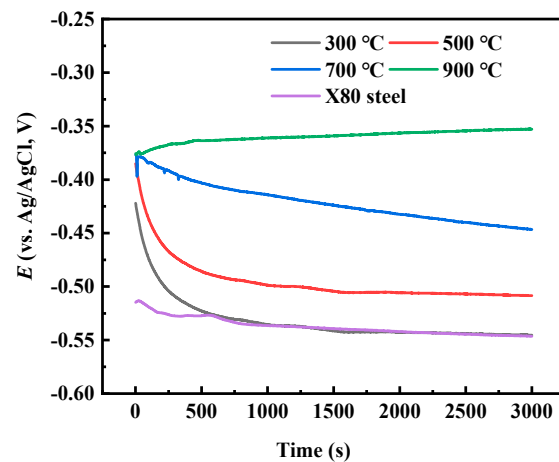


Figure 7. (a) Statistics of average friction and wear area of titanium coatings with different spraying processes; the macroscopic morphology of wear marks is as follows: (b) 300 °C, (c) 500 °C, (d) 700 °C, (e) 900 °C.

### 3.3. Simulation of Corrosion Resistance of Cold Sprayed Titanium Coatings in the Seawater Medium

Open circuit potential (OCP) testing is widely used to assess the presence of connected pores in metal coatings, displaying an OCP [45] closer to the base material. It can be seen from Figure 8 that the OCP of the C4 coating presented a slow rise, while the OCP of the C1, C2, and C3 coatings continuously decreased after the immersion test began. The OCP of the C1 coating dropped to a level close to the OCP value of the X80 steel substrate after 600 s. For the C1, C2, and C3 coatings, due to the existence of connected pores, the

corrosive medium dipped into the coating/substrate interface through the connected pores in the coating after immersion, and the highly deformed powder would be the preferred corrosion site [46]. At this time, the mixed potential between the X80 steel substrate and the outer coating exposed to the corrosive medium through the connected pores was measured.



**Figure 8.** OCP curve of unsealed coating in simulated seawater solution under different spray temperature process conditions.

The potentiodynamic polarization curve is used to evaluate the corrosion protection performance [47,48] of the metal coating. The literature has reported that the self-corrosion current density increases [49,50] with the increase in the porosity of titanium coatings. Thus, stearic acid was used to seal the coating pores in this study. The potentiodynamic polarization test results of the titanium coatings after hole sealing are shown in Figure 9. The fitting results of the potentiodynamic polarization curve are shown in Table 3. As can be seen from Figure 9, the C2, C3, and C4 curves almost coincided. This indicates that the sealing effect of the C2, C3, and C4 coatings was good, and the dimensional dull current density of the titanium coating was in the order of  $10^{-7}$   $\text{A}\cdot\text{cm}^{-2}$  [51], comparable with that of industrial pure cast titanium TA2. On the other hand, the potentiodynamic polarization curve of the C1 coating showed obvious corrosion characteristics. Its self-corrosion current density was one order of magnitude higher than that of the C4 coating, and the dimensional dull current density was still  $10^{-4}$   $\text{A}\cdot\text{cm}^{-2}$ . This indicates that even if the C1 coating with large porosity is sealed, the corrosive medium can still dip into the substrate interface and cause corrosion.

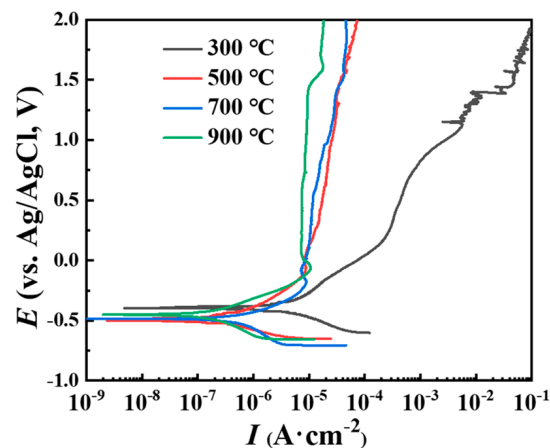


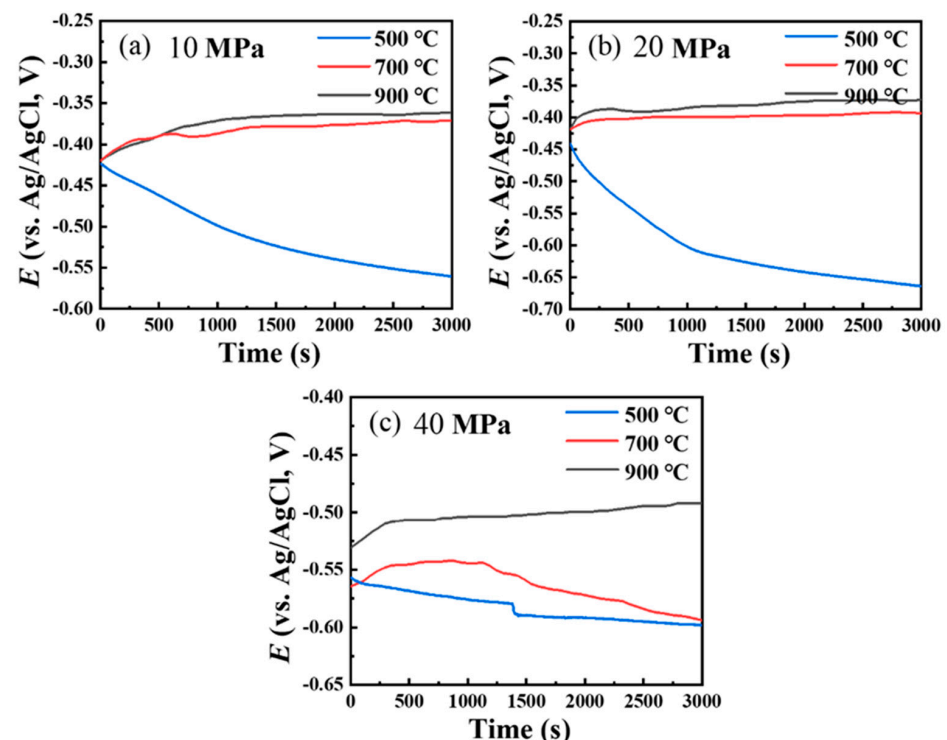
**Figure 9.** Potentiodynamic polarization curve of cold spray coating (pore sealing treatment) in simulated seawater solution.

**Table 3.** Fitting results of the potentiodynamic polarization curve of the sealed coating in 3.5 wt.% NaCl solution.

Sample	$I_{corr}$ , $A \cdot cm^{-2}$	$E_{corr}$ (V)	$I_{passive}$ ( $A \cdot cm^{-2}$ )
Sealed C1 coating	$1.23 \times 10^{-6}$	-0.672	$4.13 \times 10^{-4}$
Sealed C2 coating	$2.75 \times 10^{-7}$	-0.612	$1.75 \times 10^{-4}$
Sealed C3 coating	$4.78 \times 10^{-7}$	-0.506	$1.20 \times 10^{-5}$
Sealed C4 coating	$1.21 \times 10^{-7}$	-0.502	$8.52 \times 10^{-6}$

### 3.4. Corrosion Resistance of Cold Sprayed Titanium Coating in the Simulated Deep Sea Environment

In situ corrosion electrochemical tests were conducted on the coating after hole sealing under high hydrostatic pressure (10, 20, and 40 MPa) to characterize its corrosion resistance and further explore whether the cold sprayed titanium coating after hole sealing could meet the protection requirements of X80 steel under high hydrostatic pressure. The OCP results are shown in Figure 10. The OCP development trend of the C4 coating was the same as that of the C4 coating under 0.1 MPa, which increased slowly with the increase in the soaking time. This indicates that the corrosive medium was not immersed in the substrate interface. With the hydrostatic pressure increase from 10 to 40 MPa, the OCP of the C2 coating showed a downward trend. This was because the hydrostatic pressure led to the failure of the sealing agent, the connecting pores were re-opened, and the corrosive medium entered the coating/substrate interface. Under the hydrostatic pressure of 10 and 20 MPa, the OCP of the C3 coating increased slowly with the increase in the soaking time. When the hydrostatic pressure was 40 MPa, the OCP curve of the C3 coating increased first and then decreased. This indicates that the C3 coating could still maintain a good sealing effect at the initial immersion stage. However, with the soaking time extension, under the action of high hydrostatic pressure, the sealing material could not maintain stability, the pores were opened up, seawater entered the coating/substrate interface, and the OCP decreased.

**Figure 10.** OCP curve of sealing coating in deep sea simulated environment with different hydrostatic pressures: (a) 10 MPa; (b) 20 MPa; (c) 40 MPa.

Under different hydrostatic pressures, the potentiodynamic polarization curves of the C2, C3, and C4 coatings shifted significantly to the right in Figure 11. For the C4 coating, its potentiodynamic polarization curves under different hydrostatic pressures were very close. From the fitting results in Table 4, its self-corrosion current density increased with the increase in hydrostatic pressure. However, the increase range was small, from  $2.15 \times 10^{-7} \text{ A}\cdot\text{cm}^{-2}$  at 10 MPa hydrostatic pressure to  $4.53 \times 10^{-7} \text{ A}\cdot\text{cm}^{-2}$  at 40 MPa. Compared with the increment in the self-corrosion current density when the C2 and C3 coatings failed, the increment in the C4 coating was small. The cold sprayed titanium coating is regarded as a porous material. Since the seawater in this environment is a Newtonian fluid and the seawater penetration rate is very low, Darcy's law can describe the seawater seepage state in the coating. The high static water pressure in the deep sea environment will promote seawater penetration through the pores of the coating to the substrate interface. For the sample after sealing treatment, an overly high hydrostatic pressure may destroy the sealing structure. Thus, the pores can be re-opened, resulting in seawater entering the substrate interface and inducing corrosion.

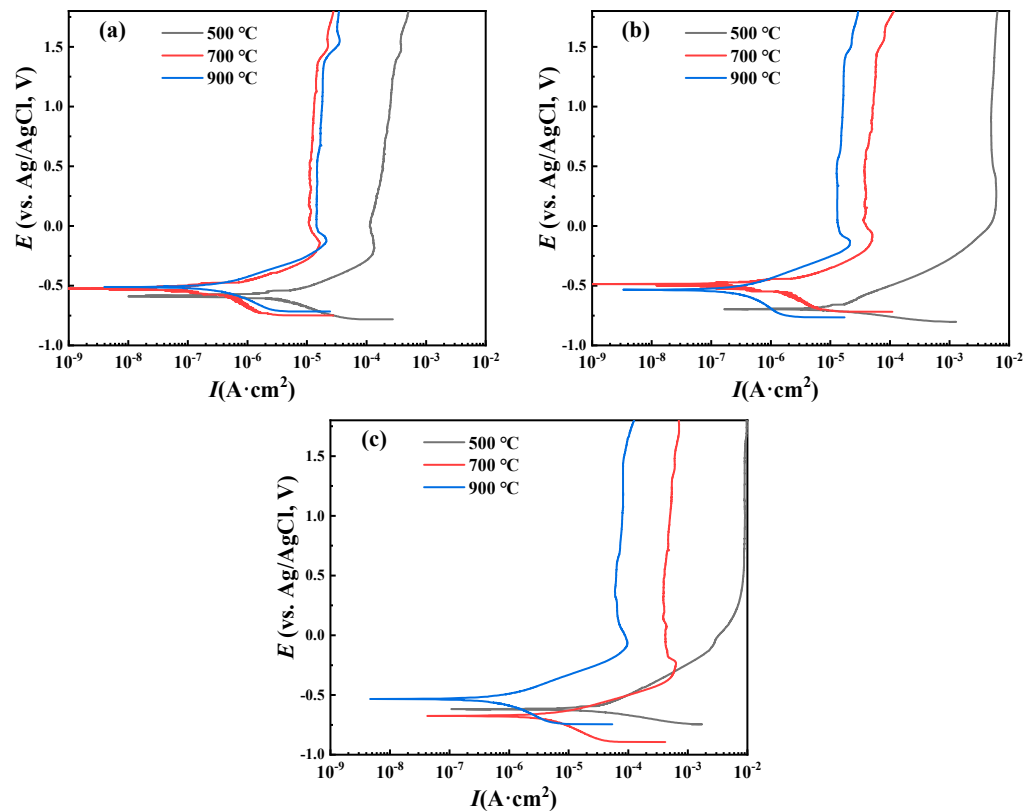


**Figure 11.** Dynamic polarization curve of sealing coating in deep sea simulated environment with different hydrostatic pressures: (a) 10 MPa; (b) 20 MPa; (c) 40 MPa.

**Table 4.** Fitting results of the self-corrosion current density of the sealing coating.

$I_{corr}$ , $\text{A}\cdot\text{cm}^{-2}$	10 MPa	20 MPa	40 MPa
Sealed C2 coating	$3.25 \times 10^{-6}$	$9.84 \times 10^{-6}$	$2.57 \times 10^{-5}$
Sealed C3 coating	$2.62 \times 10^{-7}$	$8.39 \times 10^{-7}$	$4.31 \times 10^{-6}$
Sealed C4 coating	$2.15 \times 10^{-7}$	$2.81 \times 10^{-7}$	$4.53 \times 10^{-7}$

To further determine the failure mechanism of the Ti coating under the different hydrostatic pressures, the coatings were immersed in a deep sea simulation environment under different hydrostatic pressures for 48 h to observe the cross-sectional morphology of the coating, as shown in Figure 12. Under the hydrostatic pressure of 0.1 MPa, the C1

coating had obvious corrosion cracking between the coating and the substrate. With the increase in hydrostatic pressure, the corrosion of the substrate became more serious. For the C2 coating, there was no corrosion at 0.1 MPa. When the hydrostatic pressure was increased to 10 MPa, the C2 coating showed obvious corrosion; the hydrostatic pressure was increased to 20 MPa, and the corrosion area in the C2 coating was expanded. There was an obvious hole between the coating and the substrate at 40 MPa. The C3 coating did not show corrosion under 0.1 MPa and 10 MPa. At 20 MPa, a small amount of corrosion occurred at the interface between the substrate and the coating. Compared with the C1 and C2 coatings, there was no obvious corrosion of the C3 coating. When the hydrostatic pressure was increased to 40 MPa, the corrosion was obvious and cracking occurred. The C4 coating was not corroded under the test conditions, showing good protection performance. Combined with the porosity of the coating in Figure 4, it can be seen that the sealing treatment is effective for the environment of an atmospheric pressure solution. In the environment of high hydrostatic pressure, the sealing agent will be pressed into the pores, losing its protective effect, and the solution will invade the coating, accelerating the failure of the coating. From the experimental results, it can be seen that when the coating is relatively dense, i.e., the porosity is less than 1%, the sealing treatment can effectively protect the coating from being invaded by the solution and can effectively prevent corrosion.

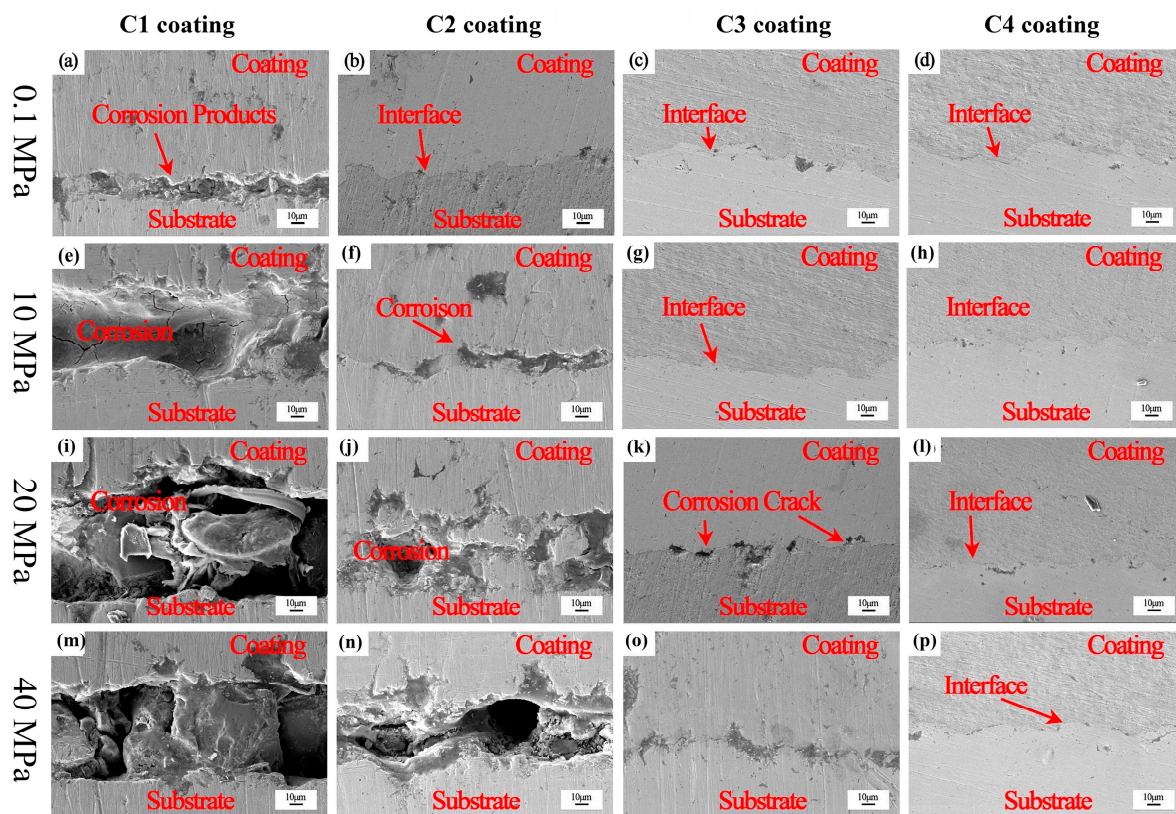


**Figure 12.** The micromorphology of the sealing coating soaked for 48 h in a deep sea simulated environment with different hydrostatic pressures: (a,e,i,m)—C1 coating; (b,f,j,n)—C2 coating; (c,g,k,o)—C3 coating; (d,h,l,p)—C4 coating.

#### 4. Conclusions

The cold sprayed titanium coating was prepared on the surface of X80 steel under different process conditions, with the adjustable carrier gas temperature as the process parameter and the irregularly shaped titanium particle powder as the raw material. The mechanical properties and corrosion protection performance in the deep sea simulated environment were tested. The results are as follows.

The composition of the cold sprayed titanium TA2 coating is mainly the  $\alpha$ -Ti phase. With an increase in the carrier gas temperature, the titanium coating becomes denser, and the porosity at a 900 °C carrier gas temperature is only 0.93%. With an increase in the carrier gas temperature, the hardness, bonding strength, and wear resistance of the cold sprayed titanium coating are improved. The bonding strength of the coating increases from 8.7 MPa at 300 °C to 46.7 MPa at 900 °C, and the hardness increases from 126 HV<sub>0.5</sub> to 247 HV<sub>0.5</sub>. Hydrostatic pressure will promote the corrosive solution to penetrate the coating with high porosity. A 500 °C or 700 °C carrier gas temperature coating can be used under normal pressure conditions, but the coating will fail under high hydrostatic pressure conditions. When the coating is sprayed at 900 °C, the dimensional blunt current density of the coating is still maintained at the order of  $10^{-7}$  A·cm<sup>-2</sup> with the commercial TA2 under the hydrostatic pressure of 40 MPa, which can be effectively protected.

**Author Contributions:** Conceptualization, Z.L., D.S. and C.X.; methodology, Z.L., N.W. and S.L.; formal analysis, Z.L. and L.W.; investigation, N.W. and S.L.; data curation, Z.L. and C.X.; writing—original draft preparation, Z.L.; writing—review and editing, N.W. and D.S. All authors have read and agreed to the published version of the manuscript.

**Funding:** This work was supported by the National Key R&D Program of China (Grant No. 2022YFA1603804), National Natural Science Foundation of China (Grant No. U21B2053) and Innovation Group Project of Southern Marine Science and Engineering Guangdong Laboratory (Zhuhai) (No. 311021013).

**Institutional Review Board Statement:** Not applicable.

**Informed Consent Statement:** Not applicable.

**Data Availability Statement:** The raw/processed data required to reproduce these findings cannot be shared at this time as the data also form part of an ongoing study.

**Acknowledgments:** Thanks associate research fellow Yibo Ai, who comes from National Center for Materials Services Safety, University of Science and Technology Beijing, and Innovation Group of Marine Engineering Materials and Corrosion Control, Southern Marine Science and Engineering Guangdong Laboratory, Zhuhai 519080, China, for her guidance on formal analysis and writing—review and editing.

**Conflicts of Interest:** The authors declare no conflict of interest. The funders had no role in the design of the study; in the collection, analyses, or interpretation of data; in the writing of the manuscript; or in the decision to publish the results.

## References

1. Liu, L.; Cui, Y.; Li, Y.; Zhang, T.; Wang, F. Failure behavior of nano-SiO<sub>2</sub> fillers epoxy coating under hydrostatic pressure. *Electrochim. Acta* **2012**, *62*, 42–50. [[CrossRef](#)]
2. Liu, Y.; Wang, J.; Liu, L.; Li, Y.; Wang, F. Study of the failure mechanism of an epoxy coating system under high hydrostatic pressure. *Corros. Sci.* **2013**, *74*, 59–70. [[CrossRef](#)]
3. Liu, B.; Fang, Z.G.; Wang, H.B.; Wang, T. Effect of cross linking degree and adhesion force on the anti-corrosion performance of epoxy coatings under simulated deep sea environment. *Prog. Org. Coat.* **2013**, *76*, 1814–1828. [[CrossRef](#)]
4. Wang, C.; Li, J.; Wang, T.; Chai, L.; Deng, C.; Wang, Y.; Huang, Y. Microstructure and properties of pure titanium coating on Ti-6Al-4V alloy by laser cladding. *Surf. Coat. Technol.* **2021**, *416*, 127137–127145. [[CrossRef](#)]
5. Song, W.W.; Feng, C.; Zhu, L.J.; Zhang, F.F. Progress of laser cladding wear resistant coating on titanium alloy surface: A review. *Mater. Sci. Forum* **2021**, *1035*, 521–527. [[CrossRef](#)]
6. Panteleenko, F.I.; Sarantsev, V.V.; Stolin, A.M.; Bazhin, P.M.; Azarenko, E.L. Formation of composite coatings based on titanium carbide via electrospark alloying. *Surf. Eng. Appl. Electrochem.* **2011**, *4*, 106–115. [[CrossRef](#)]
7. Winnicki, M.; Małachowska, A.; Baszczuk, A.; Rutkowska-Gorczyca, M.; Kukła, D.; Lachowicz, M.; Ambroziak, A. Corrosion protection and electrical conductivity of copper coatings deposited by low-pressure cold spraying. *Surf. Coat. Technol.* **2017**, *318*, 90–98. [[CrossRef](#)]
8. Wang, H.R.; Li, W.Y.; Ma, L.; Wang, J.; Wang, Q. Corrosion behavior of cold sprayed titanium protective coating on 1Cr13 substrate in seawater. *Surf. Coat. Technol.* **2007**, *201*, 5203–5216. [[CrossRef](#)]
9. DeForce, B.S.; Eden, T.J.; Potter, J.K. Cold spray Al-5% Mg coatings for the corrosion protection of magnesium alloys. *J. Therm. Spray Technol.* **2011**, *20*, 1352–1358. [[CrossRef](#)]

10. Poza, P.; Garrido-Maneiro, M.Á. Cold-sprayed coatings: Microstructure, mechanical properties, and wear behaviour. *Prog. Mater. Sci.* **2022**, *123*, 100839–100842. [[CrossRef](#)]
11. Fardan, A.; Berndt, C.C.; Ahmed, R. Numerical modelling of particle impact and residual stresses in cold sprayed coatings: A review. *Surf. Coat. Technol.* **2021**, *409*, 126835–126843. [[CrossRef](#)]
12. Klinkov, S.V.; Kosarev, V.F.; Rein, M. Cold spray deposition: Significance of particle impact phenomena. *Aerosp. Sci. Technol.* **2005**, *9*, 582–591. [[CrossRef](#)]
13. Ishikawa, K.; Suzuki, T.; Kitamura, Y.; Tobe, S. Corrosion resistance of thermal sprayed titanium coatings in chloride solution. *J. Therm. Spray Technol.* **1999**, *8*, 273–288. [[CrossRef](#)]
14. Kinos, T.; Chen, S.L.; Siitonen, P.; Kettunen, P. Densification of plasma-sprayed titanium and tantalum coatings. *J. Therm. Spray Technol.* **1996**, *5*, 439–444. [[CrossRef](#)]
15. Kinos, T.; Chen, S.L.; Siitonen, P.; Kettunen, P. Corrosion properties of shrouded plasma sprayed titanium coatings. *Therm. Spray-Curr. Status Future Trends* **1995**, *127*, 573–586.
16. Gilmore, D.L.; Dykhuizen, R.C.; Neiser, R.A.; Smith, M.F.; Roemer, T.J. Particle velocity and deposition efficiency in the cold spray process. *J. Therm. Spray Technol.* **1999**, *8*, 576–582. [[CrossRef](#)]
17. Dang, X.; Zhang, B.; Zhang, Z.; Hao, P.; Xu, Y.; Xie, Y.; Huang, R.; Wang, K.; Wang, W.; Wang, Q. Microstructural evolutions and mechanical properties of multilayered 1060Al/Al-Al<sub>2</sub>O<sub>3</sub> composites fabricated by cold spraying and accumulative roll bonding. *J. Mater. Res. Technol.* **2021**, *15*, 3895–3907. [[CrossRef](#)]
18. Lu, X.; Wang, S.; Xiong, T.; Wen, D.; Wang, G.; Du, H. Anticorrosion properties of Zn-Al-Mg-ZnO composite coating prepared by cold spraying. *Surf. Rev. Lett.* **2020**, *27*, 1950211–1950221. [[CrossRef](#)]
19. Wang, K.; Wang, S.; Xiong, T.; Wen, D.; Wang, G.; Liu, W.; Du, H. Properties of Zn-Al-Mg-TiO<sub>2</sub> coating prepared by cold spraying. *Surf. Coat. Technol.* **2020**, *387*, 125549–125553. [[CrossRef](#)]
20. Tillmann, W.; Hagen, L.; Kensy, M.D.; Abdulgader, M.; Paulus, M. Microstructural and Tribological Characteristics of Sn-Sb-Cu-Based Composite Coatings Deposited by Cold Spraying. *J. Therm. Spray Technol.* **2020**, *29*, 1027–1039. [[CrossRef](#)]
21. Wang, X.; Zhang, L.; Zhou, X.; Wu, W.; Jie, X. Corrosion behavior of Al<sub>2</sub>O<sub>3</sub>-reinforced graphene encapsulated Al composite coating fabricated by low pressure cold spraying. *Surf. Coat. Technol.* **2020**, *386*, 125486–125494. [[CrossRef](#)]
22. Winnicki, M. Advanced functional metal-ceramic and ceramic coatings deposited by low-pressure cold spraying: A Review. *Coatings* **2021**, *11*, 1044–1051. [[CrossRef](#)]
23. Wong, W.; Rezaeian, A.; Irissou, E.; Legoux, J.G.; Yue, S. Cold spray characteristics of commercially pure Ti and Ti-6Al-4V. *Adv. Mater. Res.* **2010**, *89*, 639–644. [[CrossRef](#)]
24. Meng, X.; Zhang, J.; Zhao, J.; Liang, Y.; Zhang, Y. Influence of gas Temperature on microstructure and properties of cold spray 304SS coating. *J. Mater. Sci. Technol.* **2011**, *27*, 809–815. [[CrossRef](#)]
25. Yin, S.; Suo, X.; Su, J.; Guo, Z.; Liao, H.; Wang, X. Effects of substrate hardness and spray angle on the deposition behavior of cold-sprayed Ti particles. *J. Therm. Spray Technol.* **2013**, *23*, 76–83. [[CrossRef](#)]
26. Ganesan, A.; Affi, J.; Yamada, M.; Fukumoto, M. Bonding Behavior Studies of Cold Sprayed Copper Coating on the PVC Polymer Substrate. *Surf. Coat. Technol.-Logy* **2012**, *207*, 262–269. [[CrossRef](#)]
27. Zhou, H.; Li, C.; Li, C. Research progress of titanium and titanium alloy coatings prepared by cold spraying. *China Surf. Eng.* **2020**, *33*, 1–14.
28. Wong, W.; Vo, P.; Irissou, E.; Ryabinin, A.N.; Legoux, J.G.; Yue, S. Effect of particle morphology and size distribution on cold-sprayed pure titanium coatings. *J. Therm. Spray Technol.* **2013**, *22*, 1140–1153. [[CrossRef](#)]
29. Zybala, R.; Bucholc, B.; Kaszyca, K.; Kowiorski, K.; Soboń, D.; Żórawski, W.; Moszczyńska, D.; Molak, R.; Pakieła, Z. Properties of Cold Sprayed Titanium and Titanium Alloy Coatings after Laser Surface Treatment. *Materials* **2022**, *15*, 9014. [[CrossRef](#)]
30. Boruah, D.; Zhang, X. Effect of post-deposition solution treatment and ageing on improving interfacial adhesion strength of cold sprayed Ti6Al4V coatings. *Metals* **2021**, *11*, 2038. [[CrossRef](#)]
31. Boruah, D.; McNutt, P.; Sharma, D.; Begg, H.; Zhang, X. Understanding the Effect of Substrate Preheating Temperature and Track Spacing on Laser Assisted Cold Spraying of Ti6Al4V. *Metals* **2023**, *13*, 1640. [[CrossRef](#)]
32. Tan, A.W.Y.; Sun, W.; Phang, Y.P.; Dai, M.; Marinescu, I.; Dong, Z.; Liu, E. Effects of traverse scanning speed of spray nozzle on the microstructure and mechanical properties of cold-sprayed Ti6Al4V coatings. *J. Therm. Spray Technol.* **2017**, *26*, 1484–1497. [[CrossRef](#)]
33. Tan, A.W.Y.; Sun, W.; Bhowmik, A.; Lek, J.Y.; Marinescu, I.; Li, F.; Khun, N.W.; Dong, Z.; Liu, E. Effect of coating thickness on microstructure, mechanical properties and fracture behaviour of cold-sprayed Ti6Al4V coatings on Ti6Al4V substrates. *Surf. Coat. Technol.* **2018**, *349*, 303–317. [[CrossRef](#)]
34. Sun, W.; Tan, A.W.Y.; Khun, N.W.; Marinescu, I.; Liu, E. Effect of substrate surface condition on fatigue behavior of cold sprayed Ti6Al4V coatings. *Surf. Coat. Technol.* **2016**, *320*, 452–457. [[CrossRef](#)]
35. Munagala, V.N.V.; Akinyi, V.; Vo, P.; Chromik, R.R. Influence of powder morphology and microstructure on the cold spray and mechanical properties of Ti6Al4V coatings. *J. Therm. Spray Technol.* **2018**, *27*, 827–842. [[CrossRef](#)]
36. Khun, N.W.; Tan, A.W.Y.; Bi, K.J.W.; Liu, E. Effects of working gas on wear and corrosion resistances of cold sprayed Ti-6Al-4V coatings. *Surf. Coat. Technol.* **2016**, *302*, 1–12. [[CrossRef](#)]
37. Lei, J.; Hui, P.; Wenya, L.; Xiangzhong, C.; Gang, Y. Effect of Cold Spray Parameters on Properties of TC4 Coatings. *Aerosp. Mater. Technol.* **2018**, *48*, 62–66.

38. Sun, W.; Tan, A.W.Y.; Marinescu, I.; Toh, W.Q.; Liu, E. Adhesion tribological and corrosion properties of cold sprayed CoCrMo and Ti6Al4V coating on 6061-T651 Al alloy. *Surf. Coat. Technol.* **2017**, *326*, 291–298. [[CrossRef](#)]
39. Khun, N.W.; Tan, A.W.Y.; Sun, W.; Liu, E. Wear and corrosion resistance of thick Ti-6Al-4V coating deposited on Ti-6Al-4V substrate via high-pressure cold spray. *J. Therm. Spray Technol.* **2017**, *26*, 1393–1407. [[CrossRef](#)]
40. Hao, L.; Cheng, B.R. Sealing processes of anodic coatings—Past, present, and future. *Met. Finish.* **2000**, *98*, 8–18. [[CrossRef](#)]
41. ASTM C633-01; Standard Test Method for Adhesion or Cohesion Strength of Thermal Spray Coatings. ASTM: West Conshohocken, PA, USA, 2010.
42. Li, C.J.; Li, W.Y. Deposition characteristics of titanium coating in cold spraying. *Surf. Coat. Technol.* **2003**, *167*, 278–283. [[CrossRef](#)]
43. Tushinsky, L.I.; Alkhimov, A.P.; Kosarev, V.F.; Plokhov, A.V.; Mochalina, N.S. Structure and properties of aluminum coatings obtained by the cold gas-dynamic spraying method. *Thermophys. Aeromech.* **2006**, *13*, 125–139. [[CrossRef](#)]
44. Van Steenkiste, T.H.; Smith, J.R.; Teets, R.E. Aluminum coatings via kinetic spray with relatively large powder particles. *Surf. Coat. Technol.* **2002**, *154*, 237–252. [[CrossRef](#)]
45. Hussain, T.; McCartney, D.G.; Shipway, P.H.; Marrocco, T. Corrosion behavior of cold sprayed titanium coatings and free standing deposits. *J. Therm. Spray Technol.* **2011**, *20*, 260–274. [[CrossRef](#)]
46. Zečević, S.; Dražić, D.M.; Gojković, S. Oxygen reduction on iron: Part III. An analysis of the rotating disk-ring electrode measurements in near neutral solutions. *J. Electroanal. Chem. Interfacial Electrochem.* **1989**, *265*, 179–193. [[CrossRef](#)]
47. Bolelli, G.; Lusvarghi, L.; Barletta, M. Heat treatment effects on the corrosion resistance of some HVOF-sprayed metal alloy coatings. *Surf. Coat. Technol.* **2008**, *202*, 4839–4847. [[CrossRef](#)]
48. Chidambaram, D.; Clayton, C.R.; Dorfman, M.R. Evaluation of the electrochemical behavior of HVOF-sprayed alloy coatings-II. *Surf. Coat. Technol.* **2005**, *192*, 278–283. [[CrossRef](#)]
49. Ahmed, N.; Bakare, M.S.; McCartney, D.G.; Voisey, K.T. The effects of microstructural features on the performance gap in corrosion resistance between bulk and HVOF sprayed Inconel 625. *Surf. Coat. Technol.* **2010**, *204*, 2294–2301. [[CrossRef](#)]
50. Kawakita, J.; Katanoda, H.; Watanabe, M.; Yokoyama, K.; Kuroda, S. Warm spraying: An improved spray process to deposit novel coatings. *Surf. Coat. Technol.* **2008**, *202*, 4369–4373. [[CrossRef](#)]
51. Yang, X.; Liu, Z.; Zhang, D.; Du, C.; Li, X. Stress Corrosion Cracking Behavior of Industrial Pure Titanium TA2 in Sulfide Containing Deep Seawater Environment. *China Surf. Eng.* **2019**, *32*, 17–26.

**Disclaimer/Publisher’s Note:** The statements, opinions and data contained in all publications are solely those of the individual author(s) and contributor(s) and not of MDPI and/or the editor(s). MDPI and/or the editor(s) disclaim responsibility for any injury to people or property resulting from any ideas, methods, instructions or products referred to in the content.